Materials Horizons

ROYAL SOCIETY OF CHEMISTRY

COMMUNICATION

View Article Online
View Journal | View Issue

Cite this: *Mater. Horiz.*, 2022, 9, 3048

Received 14th July 2022,
Accepted 23rd September 2022

DOI: 10.1039/d2mh00887d

rsc.li/materials-horizons

Triplet–triplet annihilation upconversion in LAPONITE®/PVP nanocomposites: absolute quantum yields of up to 23.8% in the solid state and application to anti-counterfeiting†

Lingling Wei,[a] Chunying Fan,[b] Ming Rao,[a] Fanrui Gao,[a] Cheng He,[a] Yujiao Sun,[a] Sijia Zhu,[a] Qiuhui He,[a] Cheng Yang [a] and Wanhua Wu *[a]

The low quantum efficiency in the solid phase and the highly efficient quenching by oxygen are two major weaknesses limiting the practical applications of triplet–triplet annihilation (TTA) upconversion (UC). Herein, we report an organic–inorganic hybrid nanocomposites fabricated by self-assembly of LAPONITE® clay and poly(*N*-vinyl-2-pyrrolidone) (PVP), which serves as excellent matrix for solid-state TTA-UC even in air. In the hybrid hydrogel doped by TTA-UC components, the anionic acceptors are arranged in an ordered manner at the nano-disk edge through electrostatic attraction, which avoids haphazard accumulation of the acceptors and allows for highly efficient inter-acceptor triplet energy migration. Moreover, the entangled PVP could not only protect the triplet excitons from oxygen quenching but even proactively eliminate oxygen by photoirradiation. Significantly, the dried gel prepared by completely removing water from the hydrogel gave absolute UC quantum efficiencies of up to 23.8% (out of a 50% maximum), which is the highest TTA-UC efficiency obtained in the solid state. The dried gels are readily made into powder by grinding with maintained UC emissions, making them convenient for application to information encryption and anti-counterfeiting security by virtue of the high UC quantum efficiency and insensitivity to oxygen.

New concepts

This paper reports a new record of a solid-state TTA-UC quantum yield of 23.8%, which is, to date, the only system that exceeds 20% in solid-state TTA-UC. An organic–inorganic nanocomposite was prepared by self-assembly of poly(*N*-vinyl-2-pyrrolidone) (PVP) and LAPONITE® XLG clay and was used as an excellent solid matrix for TTA-UC. The LAPONITE® clay preorganized anionic acceptors in orderly manner around the nano-disk's edges through electrostatic interaction, concentrating the acceptors without haphazard accumulation, which allowed for highly efficient inter-acceptor triplet energy migration. The entangled PVP could not only protect the triplet excitons from oxygen quenching but even proactively eliminate oxygen by photoirradiation. Thus, highly efficient TTA-UC emission in the solid state under air was observed, and the material was conveniently applied to information encryption and anti-counterfeiting security by virtue of the high UC quantum efficiency and insensitivity to oxygen.

Introduction

Triplet–triplet annihilation upconversion (TTA-UC) refers to the radiative transition of the singlet state generated by the fusion of the metastable triplets of two annihilator/emitter molecules populated *via* Dexter energy transfer (ET) from the triplets of low-energy absorbing light-harvesters/sensitizers (Fig. S1, ESI†).[1,2] By virtue of the strong oscillator strength of a singlet manifold for absorption and emission, it allows for working at subsolar irradiance power densities (~10 mW cm^{-2}) with noncoherent light and usually shows a much higher efficiency than other UC technologies.[3] Therefore, TTA-UC is highly promising for reducing the energy loss arising from the mismatch between the solar spectrum and solar cell materials and the low applicable efficiency of low-energy solar light. Together with the readily adjustable excitation and emission wavelength, TTA-UC displayed good application potentials in photovoltaics,[4,5] photocatalysis,[6–8] bioimaging,[9] and organic light-emitting diodes (OLEDs).[10,11]

Nevertheless, TTA-UC technology is still facing great challenges for practical applications. Rigorously degassing and sealing of the UC system are often required due to the high oxygen-sensitivity of long-lived triplet states.[12] Despite the superiority of TTA-UC in the solid-state over that in solutions in, for example, the convenience of processing and device manufacturing,[13] efficient TTA-UC in the solid state is quite difficult to be achieved. Extensive attempts have recently been made to exploit efficient solid-state UC systems, *e.g.* in polymer

[a] *Key Laboratory of Green Chemistry & Technology of Ministry of Education, College of Chemistry, State Key Laboratory of Biotherapy, and Healthy Food Evaluation Research Center, Sichuan University, Chengdu 610064, China. E-mail: wuwanhua@scu.edu.cn*

[b] *School of Pharmacy, Health Science Center, Xi'an Jiaotong University, Xi'an 710061, China*

† Electronic supplementary information (ESI) available. See DOI: https://doi.org/10.1039/d2mh00887d

films,[14–19] MOFs,[20–22] semi-solid materials,[23–25] elastomeric-doped matrices,[26–28] and solid crystals.[29–33] While in most cases, the UC quantum yield was less than 5% (with a theoretical maximum of 50%, similarly hereinafter), only those of a few sporadic examples exceeded 10% (Fig. S2, ESI†),[29,34] which is not satisfactory if compared to the current record of 38% obtained in solutions.[35] The limited molecular diffusion in the solid matrix that hinders the exciton delivery and inhibits the TTET and TTA processes, was the main culprit for the low UC emission in the solid-state.[19,32,36,37] Using high concentrations of UC components can sometimes improve the encountering probability and the energy transfer, but often leads to haphazard accumulation of annihilators or sensitizers due to the low dispersibility of organic molecules in the solid matrix.[38–41] Semi-solid state systems, such as gels, micelles or nanocapsules, are good candidates to achieve relatively high TTA-UC efficiencies,[42–47] in which high local concentrations, efficient triplet exciton migration, and improved oxygen tolerance due to the rigid hydrogen bonding network,[48,49] could be achieved by sophisticated structural designs. However, it also suffers from the evaporation of solvent and therefore sealing is still required for long-term use. However, while making them into solid-state films, collapsing of the assemblies occurred, which led to the reduction of the UC emission.[47] Thus, achieving efficient TTA-UC in the solvent-free solid state under air is a highly challenging task, yet is essential for the practical use of TTA-UC technology.

An ordered assembly of the sensitizers and annihilators through supramolecular aggregation could effectively avoid phase separation, and triplet energy migration among the UC components arranged in an orderly manner could efficiently transport the triplet exciton, and free itself from the constraints of molecular diffusion. Our previous studies have shown that supramolecular self-assembly of the UC components significantly improved the TTA-UC efficiencies in solution[50–52] and also proved that well-organized photosubstrates by supramolecular interactions showed unique photo-chemical and photo-physical properties.[53–62] Herein, we propose a new strategy to achieve highly efficient solid-state TTA-UC under air with an organic–inorganic nanocomposite matrix composed of poly(*N*-vinyl-2-pyrrolidone) and LAPONITE® XLG (XLG/PVP) to assemble the UC components in an ordered manner.

Results and discussion

The idea came from the unique charge-separated features of clays with positive charges at the edges and negative charges on the plate surface.[63] LAPONITE® XLG, a synthetic smectite consisting of disk-shaped particles of about 25 nm diameter and 1–2 nm thickness which self-organized into a ''house of card'' shape *via* face-edge aggregation when dispersed in water, was used as the main component of the matrix. We envisioned that the LAPONITE® clay might act as an excellent platform for pre-organizing molecules with anions around the nano-disk's edges through the electrostatic interaction and, therefore, serve to concentrate the acceptors through an orderly arrangement instead of haphazard accumulation. Thus, the frequently used

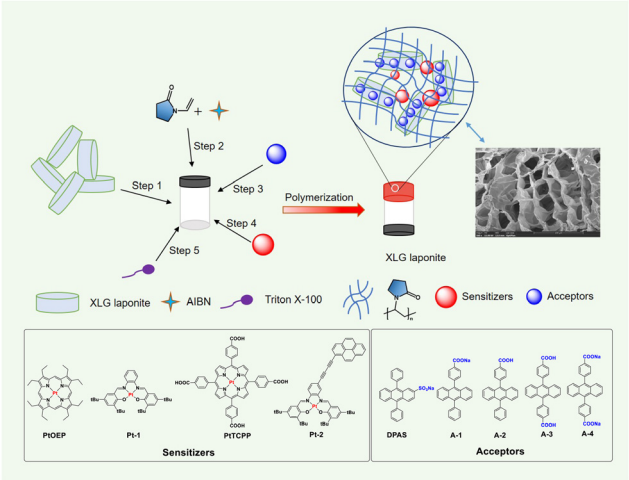

Fig. 1 The diagram of the preparation of UC XLG/PVP hydrogel and chemical structures of sensitizers and annihilators. Inset: SEM image of the UC XLG/PVP hydrogel.

triplet annihilators DPA grafted with a sulfonate anion or a carboxylic anion (**DPAS**, **A-1** and **A-4**), were used as the annihilators (Fig. 1). **A-2** and **A-3** were the corresponding acidification products of **A-1** and **A-4**. Different kinds of sensitizers with absorptions ranging from 500 to 650 nm and triplet energy levels higher than that of DPA were selected as sensitizers (Fig. 1 and ESI†). *N*-Vinyl-2-pyrrolidone (NVP), a photochemically deoxygenating solvent, was used as monomer for *in situ* radical polymerization to form poly(*N*-vinyl-2-pyrrolidone). The detailed synthesis and characterization (Fig. S4–S57, ESI†) of the UC components are shown in the ESI.†

The UC hydrogel gel was prepared as follows: the LAPONITE® colloids with a solid content of 4 wt% in deionized water was added *N*-vinyl-2-pyrrolidone (NVP) and azodiisobutyronitrile (AIBN) to give a homogeneous solution (step 1 and step 2), to which a highly concentrated DMSO solution of sensitizers and acceptors was added to form the precursor solution (step 3 and step 4), a small amount of surfactant Triton X-100 was added for better dispersion of the sensitizers in water (step 5). Heating the precursor solution at 70 °C led to the *in situ* radical polymerization of NVP initiated by AIBN with a release of nitrogen, and a transparent hydrogel with good to excellent mechanical strength was achieved after polymerizing for 10 min (Fig. 1 and Fig. S3, ESI†).[64] The hydrogen-bonding interaction between the generated poly(*N*-vinyl-2-pyrrolidone) (PVP) and the clay disks and the face-edge aggregation among the disks should be jointly responsible for the formation of the hydrogel. The scanning electron microscopy (SEM) image (Fig. 1, inset and Fig. S58, ESI†) displayed a large porous structure in the UC XLG/PVP hydrogel. The conversion rate of NVP was determined to be 29.6%, and it could be easily improved to over 90% by extending the polymerization time (Fig. S59, ESI†) but might lead to a slight decomposition of the UC components as the UC intensity slightly decreased (Fig. S79, ESI†). After a comprehensive consideration of the mechanical properties of the hydrogel, monomer conversion rate and

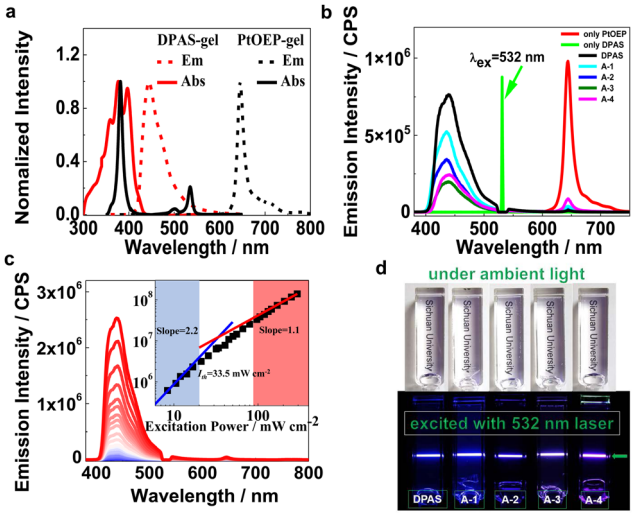

Fig. 2 (a) Normalized absorption and emission spectra of the UC dye pair in the composite hydrogel system. [**PtOEP**] = 10 μM, [**DPAS**] = 0.2 mM; (b) emission spectra of XLG/PVP gel doped with **PtOEP** only or doped with **PtOEP** as a triplet photosensitizer and **DPAS**/**A-1-A-4** as triplet acceptors under irradiation with a 532 nm laser at room temperature. A notch filter at 532 nm was used to remove the scattered incident light (power intensity (P.I.) = 8.0 mW, [**PtOEP**] = 10 μM, [**DPAS**] = 2.5 mM); (c) UC intensity of XLG/PVP gel doped with **PtOEP/DPAS** at different powers under a 532 nm laser ([**PtOEP**] = 10 μM, [**DPAS**] = 2.5 mM); inset: dependence of the integration of UC emission on the incident power density; (d) digital picture of UC hydrogel under ambient light and under irradiation of a 532 nm laser.

stability of UC components, the polymerization time was determined to be 10 min for the preparation of all the nanocomposite gels. The detailed procedures are shown in the ESI.†

The absorption and luminescence spectra of the UC dye pair of **DPAS** and **PtOEP** in the XLG/PVP hydrogel are shown in Fig. 2a. Both **PtOEP** and **DPAS** in the gel showed similar absorption spectra to those in the solution (Fig. S63–S66, ESI†), *e.g.*, distinct vibronic bands at 359 nm, 378 nm and 397 nm that corresponded to the vibration along the short axis of anthracene were observed,[65] demonstrating that the UC dye pair was molecularly dispersed in the prepared gels. Other acceptors bearing carboxylic acid or anions (**A-1-A-4**) also showed clear vibration absorption peaks (Fig. S67–S74, ESI†) in XLG/PVP hydrogel at high concentrations of 0.2 mM, and no bathochromic-shift could be observed in the fluorescence spectra if compared with that in the DMF solution, demonstrating that the XLG/PVP hydrogel could serve as an excellent matrix to disperse the acceptors nicely. The fluorescence quantum yield of the acceptors in XLG/PVP hydrogel was also determined, and high quantum yields comparable with that in the solutions were observed.[66] In particular, the quantum yield for **DPAS** in the hydrogel was as high as 92.3%, nicely satisfying the requirements of TTA-UC.

TTA-UC investigations of UC components in the XLG/PVP hydrogel were carried out under ambient conditions by using a 532 nm or 589 nm continuous diode pumped solid state (DPSS) laser. Upon irradiation of the XLG/PVP hydrogel doped with **PtOEP**, emission at 600–700 nm ascribed to the phosphorescence of **PtOEP** was observed (Fig. 2b), while in the presence of the acceptors (**DPAS**, **A-1-A-4**), the phosphorescence of **PtOEP** was almost completely quenched, but instead, a strong emission at 400–500 nm was observed. No such blue emission could be observed upon irradiation of the hydrogel doped with acceptors only, demonstrating a sensitized TTA-UC of the acceptors (Fig. 2b). The UC intensity of the acceptors **DPAS** and **A-1-A-4** sensitized by **PtOEP** in the XLG/PVP hydrogel was significantly different (Fig. 2b). The sulfonate anion grafted DPA (**DPAS**) showed the highest UC intensity under the same conditions, while **A-1** and **A-4**, with attached carboxylic anion(s), showed higher UC emission than their neutral analogues **A-2** and **A-3**, demonstrating the important role of the electrostatic interaction on the UC intensities in the present system. The UC intensity increased with the incident light power (Fig. 2c). By plotting the logarithm of UC intensity as a function of the irradiation power, a transition of slope from 2 to 1 was observed, which further confirmed the TTA-UC mechanism in the XLG/PVP hydrogels. The TTA-UC threshold excitation intensity (I_{th}) was estimated to be 33.5 mW cm^{-2} from the intersection point of the two slopes (Fig. 2c).[67] Further lowering the concentrations of **PtOEP** and **DPAS** did not significantly reduce the I_{th} (Fig. S80, ESI†), implying that the energy transfer is not diffusion-dominated.[68] The bright blue emission was readily observable under an air atmosphere with unaided eyes without any filters (Fig. 2d), indicating an efficient UC emission in this soft hydrogel. Other dye pairs showed also intense UC emission (Fig. S81–S84, ESI†).

Interestingly, we observed significant UC emission in the hydrogel prepared by the precursor solution with very low (down to 50 μM) concentrations of **DPAS** added (Fig. 3a), which is exceptional in terms of poor diffusion ability of the triplet excitons in most solid matrices, such as polymers or nanocrystals. In general, very high emitter concentrations are required to improve the TTET and TTA efficiencies, but the resulting UC efficiencies were still limited.[16,69] Upon increasing the doping amount of **DPAS** in the gels from 50 μM to 2.5 mM, the UC emission increased at the expense of the phosphorescence of **PtOEP** (Fig. 3a), and the intensity reached a plateau at a concentration higher than 2.5 mM. At the optimized conditions, the UC quantum yield of **DPAS** was up to 10.0% (Fig. 3a, inset), which is much higher than most of the currently developed UC

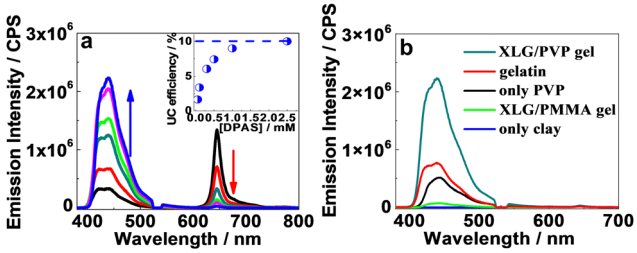

Fig. 3 (a) UC emission intensities as a function of **DPAS** concentrations in the XLG/PVP gel at room temperature ([**PtOEP**] = 10 μM); inset: UC quantum yields as a function of **DPAS** concentrations. Note: the blue arrow stands for the increase of UC intensity, and the red arrow stands for decreased the intensity of the phosphorescence of **PtOEP**. (b) UC emission intensity of 2.5 mM **DPAS** and 10 μM **PtOEP** in different hydrogels. (λ_{ex} = 532 nm, P.I. = 8 mW).

gels, *e.g.*, UC quantum yields recorded 7.5% in nanodroplet-containing polymers,[70] 7% in organogels,[46] 6.8% in gelatin,[68] and 3.5% in supramolecular gels.[71] Other acceptors **A-1-A-4** showed relatively lower UC quantum yield than **DPAS** (Table 1) but still comparable with the reported values, indicating the good performance of the present organic–inorganic nanocomposite matrix.

The efficiencies of all the involved photophysical steps of the UC systems were further analysed. As shown in Table 1, the TTET efficiency of the UC systems was almost unity for all the five acceptors. However, the parameter of Φ_{TTA} was significantly different, with anionic acceptors **A-1** and **DPAS** being much higher than others, demonstrating that regularly arraying the anionic acceptors around the clay disk was crucial for the high TTA-UC efficiencies. DPA bearing two carboxyl or carboxylic anions showed relatively lower TTA efficiencies, probably due to the crosslinking of the clays that hindered the regular assembly of acceptors.

The near unity TTET efficiency indicates that the sensitizers in the XLG/PVP hydrogels might been brought close to **DPAS** aggregates through hydrophobic and π–π interactions. Other hydrophobic sensitizers with different absorptions were also investigated (Fig. S75–S77, ESI†). With DPAS as the acceptor, good UC emission quantum yield was obtained with anti-Stokes shifts of 0.57–0.8 eV (Table S4 and Fig. S85–S87, ESI†), showing the universality of the current nanocomposite matrix. To obtain insight into the mechanism that underlies the strong TTA-UC in low dyes concentrations, zeta potential of the clay with different concentrations of **DPAS** was measured (Fig. S60, ESI†). It was found that the absolute value increased from 36.7 mV to 74.8 mV, upon increasing **DPAS** concentration from 0 mM to 2.5 mM in 4% clay solutions. The increased zeta potential demonstrated a better dispersibility of nanosheets in water which indicated that the ''house of card'' aggregations between the clays themselves collapsed after adsorbing **DPAS**.[72,73] The fluorescence wavelength showed red-shift (Fig. S61, ESI†), and the proton signals showed upfield shift upon adding the nanosheets (Fig. S62, ESI†), further verifying the assembly of **DPAS** on the edges of the LAPONITE® clay disk. Thus, the efficient UC emission at low **DPAS** loadings should be attributed to the effective concentration of the acceptors in an orderly fashion without haphazard accumulation, which ensures efficient TTET and TTA.[74]

We further compared the UC emission of different hydrogels with the same UC dye pair. As shown in Fig. 3b, when the gel was prepared with only PVP or LAPONITE® XLG as the gelator, UC emission substantially decreased or even vanished. On the other hand, only faint UC emission could be observed in the organic–inorganic nanocomposite hydrogel formed by replacing the monomer vinylpyrrolidone with methyl methacrylate, demonstrating the important role of PVP. Moreover, doping 2.5 mM **DPAS** and 11 μM **PtOEP** in gelatin hydrogel, one of the highest UC efficiency gel systems until now,[68] led to a UC intensity that is only one-third of that obtained in the XLG/PVP hydrogel. These results definitely demonstrated the excellent performance of the current nanocomposite XLG/PVP gel.

The UC emission lifetimes of the XLG/PVP hydrogel doped with **PtOEP** and **DPAS** were determined to be 2.1 ms (Fig. 4a), which is overwhelmingly longer than that of the prompt emission of **DPAS** in the hydrogel (10.7 ns, Fig. S78, ESI†) and even longer than most of the UC emission lifetimes in solution.[75,76] Considering the experiment was conducted in an unsealed cuvette and the samples were not deaerated, the long-lived UC emission verified the protection of the triplet state from oxygen quenching by the rigid hydrogen-bonding networks in this XLG/PVP gels. Moreover, the N_2 generated during the polymerization/gelation process spontaneously removed the dissolved oxygen in the aqueous phase should also be responsible.

Liquid *N*-methylpyrrolidone and PVP was reported to react with $^1O_2$ to hydroperoxide and thus can act as a photochemically deoxygenating solvent for TTA-UC.[77,78] We thus investigated the active deoxygenating function of the hydrogel XLG/PVP. The UC sample was placed in air for more than 10 days to allow adequate permeation of oxygen, and the UC emission significantly decreased compared with the incipient intensity (Fig. S88, ESI†). Interestingly, upon 532 nm laser irradiation, the UC emission gradually recovered, and the intensity was almost doubled that of the original intensity after 10 min irradiation, thereafter, the intensity kept constant upon further irradiation. No such

Table 1 The UC emission-related parameters obtained in the XLG/PVP matrix doped with different acceptors[a]

	λ_{em}[b]/nm	Φ_{UC}[c]/%	Φ_{TTET}[d]/%	Φ_{TTA}[e]/%	Φ_F[f]/%	τ[g]/ms
A-1	436	8.4	98.8	23.5	72.5	1.59
A-2	436	6.6	98.6	19.6	68.5	1.49
A-3	439	3.8	98.8	10.8	71.7	0.78
A-4	439	4.8	96.8	14.0	70.4	1.61
DPAS	427	10.0	99.7	22.0	92.3	2.1
DPAS[h]	445	23.8[i]	82.8	60.4	95.2	2.2

[a] **PtOEP** was used as a sensitizer. [b] UC emission wavelength. [c] UC quantum yields, with rhodamine B as the standard (Φ = 89% in ethanol). [d] TTET efficiency. [e] TTA efficiency. [f] Fluorescence quantum yield, with DPA as the standard (Φ = 95% in ethanol). [g] The delayed lifetime. [h] Data obtained in the solvent-free XLG/PVP dry gel. [i] Absolute UC quantum yield of the average value of five independent samples.

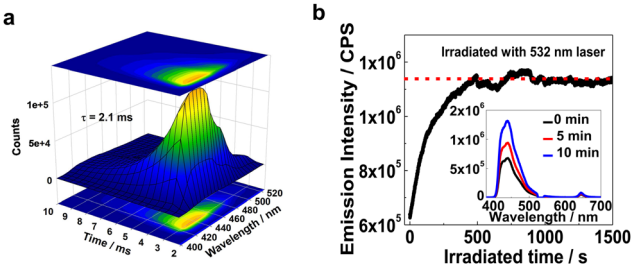

Fig. 4 (a) Time-resolved emission spectra (TRES) of the upconverted fluorescence of the XLG/PVP hydrogel at room temperature under 532 nm laser ([**PtOEP**] = 10 μM, [**DPAS**] = 2.5 mM). (b) Kinetics acquisition of the UC emission at 442 nm with continuous irradiation of 532 nm laser. The sample has been exposed to ambient atmosphere for 10 days in advance; inset: emission spectra of the UC hydrogel at different irradiation times; ([**PtOEP**] = 10 μM, [**DPAS**] = 2.5 mM, P.I. = 4.8 mW).

photo-activated kinetics process was observed for the freshly prepared hydrogel (Fig. S89, ESI†) and the XLG/PMMA gel processed with the same procedure showed only very weak increment of the incipient intensity (Fig. S90, ESI†). The polymer PVP and the residual NVP in XLG/PVP hydrogel should probably be responsible for the intensified UC emission,[77,78] leading to a first matrix that showed both positive and active protection of the UC component triplets from oxygen quenching.

The XLG/PVP UC hydrogel system worked well under a wide temperature range from −8 °C to 70 °C (Fig. S91, ESI†), which should be conducive to real-world applications. The UC emission at 70 °C decreased *ca.* 40% compared with that at 15 °C, which could be ascribed to the accelerated non-radiative inactivation of the excited state at the higher temperature, as increasing the temperature in solutions followed the same trend (Fig. S92, ESI†). The slightly increased UC intensity from 60 °C to 70 °C might be ascribed to the further polymerization of residual NVP to PVP. Continuing to raise the temperature to above 80 °C will result in opaque gels, which leads to the detection of UC emission becoming difficult (Fig. S93, ESI†). Significantly, lowering the temperature from 25 °C to −8 °C, the UC emission was only slightly decreased, which is in contrast to the drastic decrease or vanishment of UC emission commonly encountered with in soft materials under specific glass-transition temperatures (T_g) due to the restricted molecular diffusion.

The maintained TTA-UC at lower temperatures demonstrated that both TTET and TTA in such an arrangement of the sensitizers and acceptors do not require molecular diffusion for energy transfer. We, therefore, expected that the removal of the solvent should not significantly reduce the UC efficiency. Dried gels were prepared by removing water in a vacuum at 55 °C. As exemplified in Fig. 5a and b, vacuum drying of the hydrogels doped with only **PtOEP** or with **PtOEP/DPAS** produced shrunken translucent chunks. Thermogravimetric analysis (TG) showed no weight loss below 300 °C (Fig. S94, ESI†), demonstrating that no water or NVP existed in the prepared dry gels. Fourier transform infrared (FTIR) spectra showed that the UC dyes pair were successfully imbedded in the polymer framework (Fig. S95, ESI†). No glass transition temperature (T_g) was observed in the differential scanning calorimetry (DSC) curves of the XLG/PVP dried gel doped with **PtOEP** and **DPAS** (Fig. S96, ESI†), which was accordant with the fact that the UC emission did not significantly change with temperature. X-ray diffraction (XRD) spectra showed that the basal plane reflection peak at 2θ = 6.3° that corresponded to the face-to-face planar structure of LAPONITE® clay disappeared when **DPAS** was added, demonstrating that the clay lamellae delaminated into single particles and the nanosheets were well dispersed in the polymer matrix (Fig. S97, ESI†).[64] Transmission electron microscope (TEM) further confirmed this, as can be seen in Fig. 5g and h. The TEM image of the dried gel in the absence **DPAS** showed clusters of 100–300 nm, face-edge aggregations of the clays should be responsible, interestingly, the addition of **DPAS** successfully destroyed the self-assembly of nanosheets, and well-dispersed particles with an average size of 20–30 nm were observed which was in accordance with the size of a single LAPONITE® clay particle,[80]

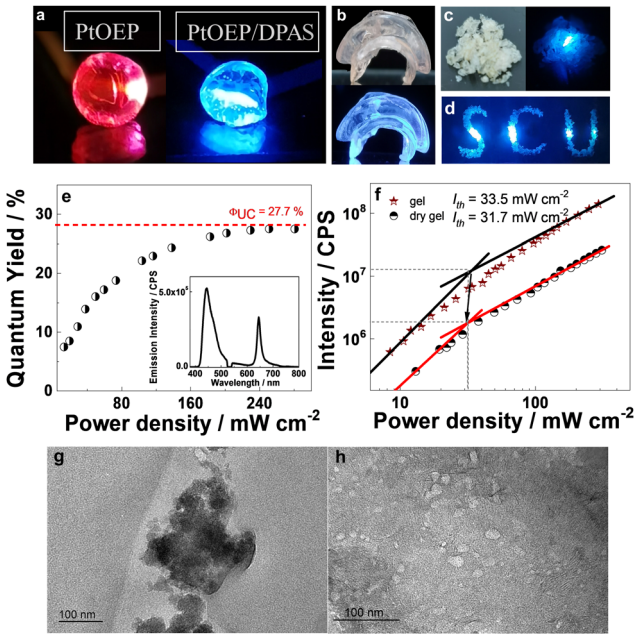

Fig. 5 Photographs of (a) the dry gel doped with **PtOEP**, **PtOEP/DPAS** with 532 nm laser, (b) the as prepared dry gel and (c) the milled powder under daylight or a 532 nm laser, and (d) arranged powder under a 532 nm laser. Note: (a–d), a 532 nm notch filter was used. (e) UC quantum yields of the dry gel as a function of incident light power density; inset: UC emission spectra of 2.5 mM **DPAS** and 10 μM **PtOEP** in the dry gel. (f) Dependence of the integration of UC emission on the incident power density of the hydrogel and dry gel. (g–h) TEM image of dried gel in the absence (g) and presence (h) of **DPAS**. ([**DPAS**] = 2.5 mM).

indicating that the annihilator loaded nanosheets may act as an independent unit for TTA-UC, which should be highly beneficent for TTA-UC in the solid matrix.

By irradiation with a 532 nm laser, the dried gel doped with **PtOEP** showed only red phosphorescence, while that doped with **PtOEP** and **DPAS** showed bright blue emission (Fig. 5a). The lifetime of the blue emission was determined to be 2.22 ms (Fig. S98, ESI†), and the intensity as a function of the irradiation power followed a first quadratic relationship and then a linear one (Fig. 5f), which jointly verified the sensitized UC emission characteristics at 400–500 nm.

The quantum efficiency of the chunk was determined with an absolute method with a fluorescence spectrophotometer equipped with an integrating sphere, and an external space laser was used as the excitation source (Fig. S99, ESI†). To reduce the negative influence of self-absorption, thin samples with a thickness of 0.5–1 mm were used, and the absorption difference between background and sample was carefully controlled to *ca.* 4–10% (Fig. S100, ESI†). Interestingly, a maximum UC quantum yield as high as 27.7% was observed as the laser power density reached 31.7 mW cm^{-2} (Fig. 5e), which, to the best of our knowledge, is the highest quantum yield ever reported in the solvent-free solid-state. Up to now, most of the UC systems in the solid state showed meager quantum yields of less than 5% (Fig. S2, ESI†) due to the limited triplet energy migration, and only sporadic examples offered Φ_{UC}

more than 10%[30,34,79] with a record of 17% in a polybutylacrilate matrix.[27]

To ensure the accuracy of the values, five independent samples that meet the criteria mentioned above were measured. The five samples showed UC quantum yield ranging 21.1–27.7%, with an absolute error of each sample below 1% (0.35–0.81%, Table S1, ESI†), the average value of the five samples was 23.8%. Decreasing the absorption difference (with thinner samples) to 0.8–1.8% did not further increase the UC quantum yield, with an average value of 22.3% in a relatively large absolute error (1.64–4.1%), demonstrating that the samples with absorption difference of 4–10% was appropriate for quantum yield measurements. A relative method was further applied to determine the UC quantum yield with the emission of **PtOEP** embedded in the same matrix as the standard (please refer to the ESI† for a detailed description of the experiment), and the average quantum yield of ten independent samples was determined to be 23.6% which was very close to that determined using an absolute method, demonstrating the reliability of our methods.

In order to precisely confirm the average ratio of acceptor molecules adsorbed per nanoparticle and get more insight into the efficient TTA-UC in the current solid matrix, the adsorption behaviour of anionic **DPAS** onto the LAPONITE® surface was studied (Fig. S102, ESI†). It was interesting to find that the maximum adsorption capacity of **DPAS** by nanosheets was determined to be as high as 19.7 mg g^{-1}, which is much higher than that of other negatively charged agents.[81] Besides the electrostatic interaction between the anionic **DPAS** and the positively charged edges of the platelets, the hydrophobic inter-DPA stacking should also be responsible for the large adsorbing amount, which could minimize their hydrophobic surface exposed to the aqueous medium.[81]

The average ratio of acceptor molecules adsorbed by per nanosheet was calculated according to the adsorption amount (refer to the ESI† for calculation detail). The ratio was determined to be (112–119) : 1, from which the average inter-DPA distance at the nanosheet was estimated to be 8.2 Å, which was significantly shorter than the effective triplet–triplet interaction distance of 9.1 Å for DPA.[82] Such a short inter-DPA distance indicated that **DPAS** might be tightly arranged, and the π-plane of anthracene in **DPAS** has to be parallelly assembled around the edge of nano-disk (Fig. S101, ESI†), which results in weakly exchange-coupled triplet-pair states that lead to a higher spin-statistical value (η) than normal TTA-UC systems,[26] to finally give a high quantum yield that even exceeded the statistical limit of 20%.

The hydrogel could be easily processed into different shapes and converted into the corresponding dry gel, *e.g.*, a jellyfish-shaped dry gel with different thicknesses at different body parts was thus prepared, and the blue UC emission was not apparently influenced by the thickness of the UC material (Fig. 5b). Moreover, grinding the UC chunk into granuloma (Fig. 5c and d) did not influence the UC quantum yield, demonstrating the excellent machinability characteristics of the UC XLG/PVP material. This further provides the possibility of the convenient use of UC powder to fabricate materials with different shapes.

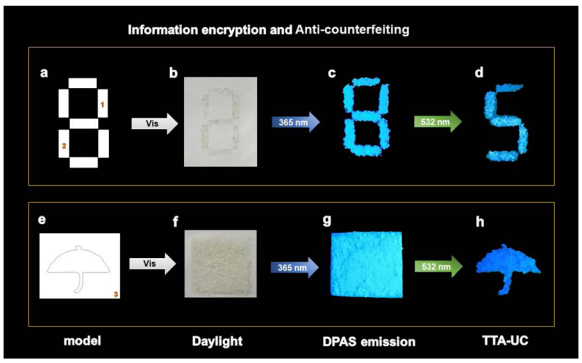

Fig. 6 Information encryption and anti-counterfeiting applications of solid-state TTA-UC. (a and e) The models. (b–d, f–g) Photographs of the patterns under ambient light (b and f), 365 nm (c and g) and 532 nm light (d and h) irradiation, respectively. The encrypted number "5" and "umbrella" patterns can be observed only under 532 nm excitation. Note: (d and h), a 532 nm notch filter was used.

The highly efficient UC emission under ambient conditions led us to investigate the applications of this material. For the sake of operation convenience, we grind the dried gel into fine powder. It turned out that the powders showed UC emission under 532 nm irradiation wherever it was scattered, making these materials extremely appealing for practical applications. As a conceptual illustration, we applied the material in the field of information encryption and anti-counterfeiting technique. Thus, self-made models were filled with the mashed XLG/PVP powders containing only **DPAS** (the part labelled with numbers 1–3) or UC dye pair of **DPAS/PtOEP** (the remaining parts not labelled). As is shown in Fig. 6, the two different materials were all white powders under ambient light (Fig. 6b and f). Under 365 nm irradiation, the patterns showed bright blue emissions (Fig. 6c and g), and the designed pattern (5 and umbrella) was encrypted. Only when the patterns were irradiated with a 532 nm laser, the encrypted number "5" and pattern "umbrella" could be decoded (Fig. 6d and h), showing an excellent double anti-counterfeiting function of these materials. It should be pointed out that benefiting from the low threshold excitation intensity of these materials, we expanded the spot of 532 nm laser from 1 mm to 7.5 cm, with power density as low as 1.13 mW cm^{-2}, and the encrypted patterns were eye-catching with the aid of only a notch filter to remove the scattering laser. The expanded spot will show much higher efficiency for decoding when compared with that of point-by-point scanning commonly required for TTA-UC emission, demonstrating the excellent performance of these materials in practical applications.

Conclusions

In conclusion, organic–inorganic nanocomposites comprising of poly(*N*-vinyl-2-pyrrolidone) and LAPONITE® were demonstrated to be an excellent matrix for highly efficient TTA upconversion as a result of well-organized acceptors and sensitizers around the edges of the LAPONITE® disk. The nanocomposite

hydrogels can protect the triplets of the UC components from oxygen quenching, even showing effective deoxygenation ability through photoirradiation. Significantly, the dried gels achieved by removing water of the hydrogel exhibit extremely high UC emission with absolute UC quantum efficiency of as high as 23.8%, which is so far the highest UC quantum efficiency observed in the solid state. The dried gel showed excellent machinability characteristics, and the finely ground powder still showed bright UC emission under air, which was successfully applied to information encryption and anti-counterfeiting security. This study paved a new way of arranging the UC components in the solid state to facilitate energy transfer, and the extremely high UC efficiency makes the system closer to the practical application of TTA-UC.

Author contributions

L. W., C. Y. and W. W. conceived the ideas and designed the experiments, analyzed the data, and prepared the manuscript, with input from all the authors. L. W. performed the chemical synthesis and UC measurements. C. F., M. R., F. G., C. H., Y. S., S. Z. and Q. H. gave advice on UC emission measurements. All authors contributed to discussion and analysis of the data.

Conflicts of interest

There are no conflicts to declare.

Acknowledgements

We acknowledge the support of this work by the National Natural Science Foundation of China (No. 22171194, 21971169, 92056116, 21871194, and 21572142), the National Key Research and Development Program of China (NKRDPC, No. 2017YFA0505903), the Science & Technology Department of Sichuan Province (2022YFH0095 and 2021ZYD0052). Material characterizations were performed with the support of the Comprehensive Training Platform of Specialized Laboratory, College of Chemistry, Professor Peng Wu and Hui Wang of the Analytical & Testing Center, Sichuan University, which were greatly appreciated.

Notes and references

1 T. N. Singh-Rachford and F. N. Castellano, *Coord. Chem. Rev.*, 2010, **254**, 2560–2573.
2 J. Zhao, S. Ji and H. Guo, *RSC Adv.*, 2011, **1**, 937–950.
3 J. Zhou, Q. Liu, W. Feng, Y. Sun and F. Li, *Chem. Rev.*, 2015, **115**, 395–465.
4 B. S. Richards, D. Hudry, D. Busko, A. Turshatov and I. A. Howard, *Chem. Rev.*, 2021, **121**, 9165–9195.
5 V. Gray, D. Dzebo, M. Abrahamsson, B. Albinsson and K. Moth-Poulsen, *Phys. Chem. Chem. Phys.*, 2014, **16**, 10345–10352.
6 M. Rao, K. Kanagaraj, C. Fan, J. Ji, C. Xiao, X. Wei, W. Wu and C. Yang, *Org. Lett.*, 2018, **20**, 1680–1683.
7 M. Rao, W. Wu and C. Yang, *Molecules*, 2019, **24**, 1502.
8 M. Rao, C. Fan, J. Ji, W. Liang, L. Wei, D. Zhang, Z. Yan, W. Wu and C. Yang, *ACS Appl. Mater. Interfaces*, 2022, **14**, 21453–21460.
9 P. Peng, N. Wu, L. Ye, F. Jiang, W. Feng, F. Li, Y. Liu and M. Hong, *ACS Nano*, 2020, **14**, 16672–16680.
10 C. Lin, P. Han, F. Qu, S. Xiao, Y. Li, D. Xie, X. Qiao, D. Yang, Y. Dai, Q. Sun, A. Qin, B. Z. Tang and D. Ma, *Mater. Horiz.*, 2022, **9**, 2376–2383.
11 P. Han, C. Lin, K. Wang, Y. Qiu, H. Wu, A. Qin, D. Ma and B. Z. Tang, *Mater. Horiz.*, 2022, **9**, 376–382.
12 R. S. Khnayzer, J. Blumhoff, J. A. Harrington, A. Haefele, F. Deng and F. N. Castellano, *Chem. Commun.*, 2012, **48**, 209–211.
13 T. A. Lin, C. F. Perkinson and M. A. Baldo, *Adv. Mater.*, 2020, **32**, 1908175.
14 N. Yanai and N. Kimizuka, *Chem. Commun.*, 2016, **52**, 5354–5370.
15 T. Kashino, M. Hosoyamada, R. Haruki, N. Harada, N. Yanai and N. Kimizuka, *ACS Appl. Mater. Interfaces*, 2021, **13**, 13676–13683.
16 S. Raišys, O. Adomėnienė, P. Adomėnas, A. Rudnick, A. Köhler and K. Kazlauskas, *J. Phys. Chem. C*, 2021, **125**, 3764–3775.
17 A. Turshatov, D. Busko, N. Kiseleva, S. L. Grage, I. A. Howard and B. S. Richards, *ACS Appl. Mater. Interfaces*, 2017, **9**, 8280–8286.
18 S. Raisys, K. Kazlauskas, S. Jursenas and Y. C. Simon, *ACS Appl. Mater. Interfaces*, 2016, **8**, 15732–15740.
19 F. Marsico, A. Turshatov, R. Pekoz, Y. Avlasevich, M. Wagner, K. Weber, D. Donadio, K. Landfester, S. Baluschev and F. R. Wurm, *J. Am. Chem. Soc.*, 2014, **136**, 11057–11064.
20 S. Gharaati, C. Wang, C. Forster, F. Weigert, U. Resch-Genger and K. Heinze, *Chemistry*, 2020, **26**, 1003–1007.
21 F. Meinardi, M. Ballabio, N. Yanai, N. Kimizuka, A. Bianchi, M. Mauri, R. Simonutti, A. Ronchi, M. Campione and A. Monguzzi, *Nano Lett.*, 2019, **19**, 2169–2177.
22 P. Mahato, A. Monguzzi, N. Yanai, T. Yamada and N. Kimizuka, *Nat. Mater.*, 2015, **14**, 924–930.
23 T. Mizokuro, A. Abulikemu, K. Suzuki, Y. Sakagami, R. Nishii, T. Jin and K. Kamada, *Phys. Chem. Chem. Phys.*, 2020, **22**, 17807–17813.
24 P. Bharmoria, S. Hisamitsu, Y. Sasaki, T. S. Kang, M.-a Morikawa, B. Joarder, K. Moth-Poulsen, H. Bildirir, A. Mårtensson, N. Yanai and N. Kimizuka, *J. Mater. Chem. C*, 2021, **9**, 11655–11661.
25 F. Saenz, A. Ronchi, M. Mauri, R. Vadrucci, F. Meinardi, A. Monguzzi and C. Weder, *Adv. Funct. Mater.*, 2020, **31**, 2004595.
26 D. G. Bossanyi, Y. Sasaki, S. Wang, D. Chekulaev, N. Kimizuka, N. Yanai and J. Clark, *JACS Au*, 2021, **1**, 2188–2201.
27 A. Monguzzi, F. Bianchi, A. Bianchi, M. Mauri, R. Simonutti, R. Ruffo, R. Tubino and F. Meinardi, *Adv. Energy Mater.*, 2013, **3**, 680–686.

28 M. Samiullah, D. Moghe, U. Scherf and S. Guha, *Phys. Rev. B*, 2010, **82**, 205211.
29 R. Enomoto, M. Hoshi, H. Oyama, H. Agata, S. Kurokawa, H. Kuma, H. Uekusa and Y. Murakami, *Mater. Horiz.*, 2021, **8**, 3449–3456.
30 K. Kamada, Y. Sakagami, T. Mizokuro, Y. Fujiwara, K. Kobayashi, K. Narushima, S. Hirata and M. Vacha, *Mater. Horiz.*, 2017, **4**, 83–87.
31 M. Hosoyamada, N. Yanai, T. Ogawa and N. Kimizuka, *Chemistry*, 2016, **22**, 2060–2067.
32 M. Wu, D. N. Congreve, M. W. B. Wilson, J. Jean, N. Geva, M. Welborn, T. Van Voorhis, V. Bulović, M. G. Bawendi and M. A. Baldo, *Nat. Photonics*, 2015, **10**, 31–34.
33 A. Ronchi, C. Capitani, V. Pinchetti, G. Gariano, M. L. Zaffalon, F. Meinardi, S. Brovelli and A. Monguzzi, *Adv. Mater.*, 2020, **32**, 2002953.
34 J.-H. Kim, F. Deng, F. N. Castellano and J.-H. Kim, *Chem. Mater.*, 2012, **24**, 2250–2252.
35 S. Hoseinkhani, R. Tubino, F. Meinardi and A. Monguzzi, *Phys. Chem. Chem. Phys.*, 2015, **17**, 4020–4024.
36 A. Abulikemu, Y. Sakagami, C. Heck, K. Kamada, H. Sotome, H. Miyasaka, D. Kuzuhara and H. Yamada, *ACS Appl. Mater. Interfaces*, 2019, **11**, 20812–20819.
37 X. Jiang, X. Guo, J. Peng, D. Zhao and Y. Ma, *ACS Appl. Mater. Interfaces*, 2016, **8**, 11441–11449.
38 C. Ye, J. Ma, S. Chen, J. Ge, W. Yang, Q. Zheng, X. Wang, Z. Liang and Y. Zhou, *J. Phys. Chem. C*, 2017, **121**, 20158–20164.
39 T. Ogawa, M. Hosoyamada, B. Yurash, T. Q. Nguyen, N. Yanai and N. Kimizuka, *J. Am. Chem. Soc.*, 2018, **140**, 8788–8796.
40 T. Ogawa, N. Yanai, S. Fujiwara, T.-Q. Nguyen and N. Kimizuka, *J. Mater. Chem. C*, 2018, **6**, 5609–5615.
41 E. Radiunas, M. Dapkevicius, S. Raisys, S. Jursenas, A. Jozeliunaite, T. Javorskis, U. Sinkeviciute, E. Orentas and K. Kazlauskas, *Phys. Chem. Chem. Phys.*, 2020, **22**, 7392–7403.
42 D. F. Barbosa de Mattos, A. Dreos, M. D. Johnstone, A. Runemark, C. Sauvee, V. Gray, K. Moth-Poulsen, H. Sunden and M. Abrahamsson, *J. Chem. Phys.*, 2020, **153**, 214705.
43 P. Bharmoria, N. Yanai and N. Kimizuka, *Gels*, 2019, **5**, 18.
44 X. Liu, J. Fei, P. Zhu and J. Li, *Chem. – Asian J.*, 2016, **11**, 2700–2704.
45 K. Sripathy, R. W. MacQueen, J. R. Peterson, Y. Y. Cheng, M. Dvořák, D. R. McCamey, N. D. Treat, N. Stingelin and T. W. Schmidt, *J. Mater. Chem. C*, 2015, **3**, 616–622.
46 T. Ogawa, N. Yanai, A. Monguzzi and N. Kimizuka, *Sci. Rep.*, 2015, **5**, 10882.
47 H. Kouno, T. Ogawa, S. Amemori, P. Mahato, N. Yanai and N. Kimizuka, *Chem. Sci.*, 2016, **7**, 5224–5229.
48 R. Vadrucci, C. Weder and Y. C. Simon, *Mater. Horiz.*, 2015, **2**, 120–124.
49 Y. Murakami, Y. Himuro, T. Ito, R. Morita, K. Niimi and N. Kiyoyanagi, *J. Phys. Chem. B*, 2016, **120**, 748–755.
50 C. Fan, W. Wu, J. J. Chruma, J. Zhao and C. Yang, *J. Am. Chem. Soc.*, 2016, **138**, 15405–15412.
51 H. Lai, T. Zhao, Y. Deng, C. Fan, W. Wu and C. Yang, *Chin. Chem. Lett.*, 2019, **30**, 1979–1983.
52 Q. Guo, G. Li, M. Rao, L. Wei, F. Gao, W. Wu, Q. Yang, G. Cheng and C. Yang, *Dyes Pigm.*, 2020, **182**, 108643.
53 J. Song, H. Xiao, L. Fang, L. Qu, X. Zhou, Z.-X. Xu, C. Yang and H. Xiang, *J. Am. Chem. Soc.*, 2022, **144**, 2233–2244.
54 C. Tu, W. Wu, W. Liang, D. Zhang, W. Xu, S. Wan, W. Lu and C. Yang, *Angew. Chem., Int. Ed.*, 2022, **61**, e202203541.
55 J. Yao, W. Wu, C. Xiao, D. Su, Z. Zhong, T. Mori and C. Yang, *Nat. Commun.*, 2021, **12**, 2600.
56 Y. Mi, J. Ma, W. Liang, C. Xiao, W. Wu, D. Zhou, J. Yao, W. Sun, J. Sun, G. Gao, X. Chen, J. J. Chruma and C. Yang, *J. Am. Chem. Soc.*, 2021, **143**, 1553–1561.
57 C. Xiao, W. Wu, W. Liang, D. Zhou, K. Kanagaraj, G. Cheng, D. Su, Z. Zhong, J. J. Chruma and C. Yang, *Angew. Chem., Int. Ed.*, 2020, **59**, 8094–8098.
58 X. Wei, J. Liu, G.-J. Xia, J. Deng, P. Sun, J. J. Chruma, W. Wu, C. Yang, Y.-G. Wang and Z. Huang, *Nat. Chem.*, 2020, **12**, 551–559.
59 J. Ji, W. Wu, W. Liang, G. Cheng, R. Matsushita, Z. Yan, X. Wei, M. Rao, D.-Q. Yuan, G. Fukuhara, T. Mori, Y. Inoue and C. Yang, *J. Am. Chem. Soc.*, 2019, **141**, 9225–9238.
60 C. Fan, L. Wei, T. Niu, M. Rao, G. Cheng, J. J. Chruma, W. Wu and C. Yang, *J. Am. Chem. Soc.*, 2019, **141**, 15070–15077.
61 X. Wei, W. Wu, R. Matsushita, Z. Yan, D. Zhou, J. J. Chruma, M. Nishijima, G. Fukuhara, T. Mori, Y. Inoue and C. Yang, *J. Am. Chem. Soc.*, 2018, **140**, 3959–3974.
62 F. Gao, X. Yu, L. Liu, J. Chen, Y. Lv, T. Zhao, J. Ji, J. Yao, W. Wu and C. Yang, *Chin. Chem. Lett.*, 2022, DOI: **10.1016/j.cclet.2022.05.072**.
63 S. Miyazaki, H. Endo, T. Karino, K. Haraguchi and M. Shibayama, *Macromolecules*, 2007, **40**, 4287–4295.
64 K. Park, J. I. Dawson, R. O. C. Oreffo, Y. H. Kim and J. Hong, *Biomacromolecules*, 2020, **21**, 2096–2103.
65 C. Peng, W. Liang, J. Ji, C. Fan, K. Kanagaraj, W. Wu, G. Cheng, D. Su, Z. Zhong and C. Yang, *Chin. Chem. Lett.*, 2021, **32**, 345–348.
66 J. V. Morris, M. A. Mahaney and J. R. Huber, *J. Phys. Chem.*, 1976, **80**, 969–974.
67 W. Xu, W. Liang, W. Wu, C. Fan, M. Rao, D. Su, Z. Zhong and C. Yang, *Chem. – Eur. J.*, 2018, **24**, 16677–16685.
68 P. Bharmoria, S. Hisamitsu, H. Nagatomi, T. Ogawa, M. A. Morikawa, N. Yanai and N. Kimizuka, *J. Am. Chem. Soc.*, 2018, **140**, 10848–10855.
69 R. R. Islangulov, J. Lott, C. Weder and F. N. Castellano, *J. Am. Chem. Soc.*, 2007, **129**, 12652–12653.
70 R. Vadrucci, A. Monguzzi, F. Saenz, B. D. Wilts, Y. C. Simon and C. Weder, *Adv. Mater.*, 2017, **29**, 1702992.
71 P. Duan, N. Yanai, H. Nagatomi and N. Kimizuka, *J. Am. Chem. Soc.*, 2015, **137**, 1887–1894.
72 A. Pek-Ing and L. Yee-Kwong, *Appl. Clay Sci.*, 2015, **107**, 36–45.
73 Y. Liu, M. Zhu, X. Liu, W. Zhang, B. Sun, Y. Chen and H. P. Adler, *Polymer*, 2006, **47**, 1–5.
74 N. Kimizuka, N. Yanai and M. A. Morikawa, *Langmuir*, 2016, **32**, 12304–12322.
75 A. Olesund, V. Gray, J. Mårtensson and B. Albinsson, *J. Am. Chem. Soc.*, 2021, **143**, 5745–5754.
76 A. J. Tilley, B. E. Robotham, R. P. Steer and K. P. Ghiggino, *Chem. Phys. Lett.*, 2015, **618**, 198–202.

77 J. Lin, S. Wan, W. Liu and W. Lu, *Chem. Commun.*, 2019, **55**, 4299–4302.
78 S. Wan, J. Lin, H. Su, J. Dai and W. Lu, *Chem. Commun.*, 2018, **54**, 3907–3910.
79 A. Monguzzi, M. Mauri, A. Bianchi, M. K. Dibbanti, R. Simonutti and F. Meinardi, *J. Phys. Chem. C*, 2016, **120**, 2609–2614.
80 K. Haraguchi, R. Farnworth, A. Ohbayashi and T. Takehisa, *Macromolecules*, 2003, **36**, 5736–5741.
81 T. C. Chaparro, R. D. Silva, I. S. Monteiro, A. Barros-Timmons, R. Giudici, A. M. Santos and E. Bourgeat-Lami, *Langmuir*, 2019, **35**, 11512–11523.
82 A. Monguzzi, J. Mezyk, F. Scotognella, R. Tubino and F. Meinardi, *Phys. Rev. B*, 2008, **78**, 195112.

